J. Fluid Mech. (1977), *vol.* 81, *part* 2, *pp.* 225–240
Printed in Great Britain

Doppler measurements of the effects of gravity waves on wind-generated ripples

By PETER H. Y. LEE

Engineering Sciences Laboratory, TRW/DSSG,
One Space Park, Redondo Beach, California 90278†

(Received 2 March 1976)

The effects of gravity waves on wind-generated ripples are studied experimentally by means of Doppler spectra obtained through microwave Bragg backscattering. The measurements were made at 9·23 GHz with incidence angles of between 45° and 55°. It is found from the Doppler frequency shift that an increase in the speed of Bragg waves (ripples) of wavelength approximately 2 cm can be detected when a gravity wave is propagated into a pre-existing wind-wave field. The Doppler frequency shift corresponds, to first order, to the orbital speed of the gravity wave. Further studies, using a conditional sampling technique, reveal that the Bragg scatterers are localized on the gravity wave's crest. The mechanism leading to the 'localization' is as yet unidentified. Ratios of gravity wavelength to Bragg (ripple) wavelength ranging from 13 to 35 have been studied.

1. Introduction

In the past few years, many wind-wave studies have been performed by using microwave diagnostics both in the ocean as well as in the laboratory. It is well known that, for wind-wave surfaces which fall into the 'slightly rough' or 'composite surface' categories (Rice 1951; Peake 1959; Semyonov 1966; Wright 1968; Bass *et al.* 1968; Valenzuela 1968), Bragg scattering, first identified by Crombie (1955), is the primary scattering mechanism for radar returns. From direct measurements of Doppler spectra of any given wind-wave field, the mean speed of the Bragg-resonant water wave (or, simply, the Bragg wave) can be obtained (Pidgeon 1968; Valenzuela & Laing 1970; Wright & Keller 1971; Duncan, Keller & Wright 1974). The Bragg wave speed consists of the phase speed of the water wave whose wavelength satisfies the Bragg resonance condition plus contributions or 'modifications' due to the wind-induced drift current and, for cases where the wavelength of the Bragg scatterers is much shorter than the wavelength of the dominant wave, the dominant waves' orbital velocity. For radar backscattering the latter contribution is, however, not well understood and even subject to some confusion.

In general, even the more deterministic case of the effects produced by mechanically generated gravity waves interacting with shorter gravity–capillary waves in the presence of a wind-induced current field is still a problem not completely understood, although the problem of short waves riding on longer gravity waves has been studied

† Present address: University of California, Lawrence Livermore Laboratory, P.O. Box 808, Mail Station L-549, Livermore, California 94550.

by several authors (Unna 1941, 1942, 1947; Cox 1958; Longuet-Higgins & Stewart 1960).

A good summary of the theoretical results on the interaction of short waves with long waves can be found in Longuet-Higgins & Stewart (1960). The essential feature of the nonlinear interaction between short waves and long waves can be characterized by the radiation stress, which results in the fact that shorter gravity waves have a tendency to become both shorter and steeper at the crests of the longer waves, and correspondingly longer and lower in the troughs. An estimate of the magnitude of the shortening (of wavelength) and steepening of the short waves is given by the value of ka for the long waves.

In an attempt to gain a better understanding of the effects of gravity waves on wind waves, a specific case of the effects of gravity waves on shorter gravity–capillary waves (ripples of wavelength approximately 2 cm) is studied under controlled laboratory conditions. The experimental configuration is produced in a wind-tunnel/wave-tank facility in which a mechanically generated gravity wave is propagated into a pre-existing wind-wave field. The effects of the gravity wave on wind-generated ripples are obtained from measurements of the Doppler spectrum by means of an X-band ($\lambda_0 = 3{\cdot}25$ cm) radar system. In the present case, the ripples (wavelength ~ 2 cm) are shorter than the wind-generated dominant wave (wavelength ~ 8 cm), whereas the mechanically generated gravity waves (wavelength $30 \sim 70$ cm) are much longer than the dominant wave.

In this paper, results of the effects of gravity waves on the measured Bragg wave speed are presented for ratios of gravity wavelength to Bragg wavelength in the range 13–35. It is found that, when a gravity wave is superimposed on a wind wave, an increase in Doppler frequency (i.e. an increase in the Bragg wave speed) can be measured. The increase in the Bragg wave speed is of the same magnitude as the orbital speed of the gravity wave. This leads one to hypothesize that, through some interaction of the gravity wave with the wind wave, the ripples are 'localized' on the crest of the gravity wave. A conditional sampling technique is then devised and implemented to sample microwave returns from specific portions of the gravity wave. It is found that the hypothesis is correct, i.e. the ripples are located predominantly on the crest of the gravity wave.

It should be pointed out that the present experimental inquiry was not designed to test the validity of the widely accepted results of Longuet-Higgins & Stewart. However, it is important to note that none of the results implied by the microwave Doppler returns indicate any contradictions with their general theory. This will be discussed in the last section.

2. Experimental facilities and equipment

The experiments were performed in the TRW/ESL Wave Tank Facility. The tank is a $0{\cdot}914 \times 0{\cdot}914 \times 12{\cdot}2$ m glass and steel structure designed to generate surface waves. An open-circuit wind tunnel is located over the entire length of the tank to provide for wave interaction studies in which surface waves are generated by wind. Microwave scattering measurements are made while the surface waves propagate from one end of the tank, where they are generated by a programmable wave maker or by wind, to the opposite end of the tank, where they are effectively absorbed by a shallow-

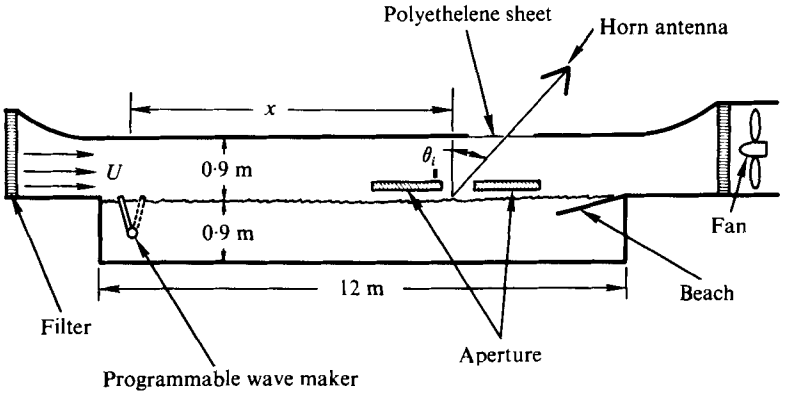

FIGURE 1. Schematic diagram of wave-tank/wind-tunnel facility.

angle beach. The wave tank is described in detail in Lewis, Lake & Ko (1974). The programmable wave maker is described in detail in Yuen & Lake (1975).

The wind-wave generation system is basically an open-circuit wind tunnel installed over the upper water surface of the wave tank (see figure 1). The major system components are an inlet contraction section located over the wave-maker end of the tank, a 12·2 m test section over the working section of the tank, and a diffuser and fan located downwind of the wave-absorber end of the tank. The direction of air flow is from the wave-maker end of the tank to the wave-absorber end. The fan has been placed at the downwind end of the system in order to avoid the swirl velocities which generate cross-flow of wind and waves in wind-wave tanks where fans are located at the upstream end. The inlet contraction section contains air filters and screens to ensure that the incoming air flow is clean and has low turbulence levels. Preliminary measurements indicate that turbulence levels are no more than a few per cent. The test section over the 12·2 m working section of the tank extends across the full width of the tank and is currently set to provide a 0·914 m test-section height above the water surface. The inlet, test section and diffuser are designed to permit considerable variation of tunnel geometry. In the present configuration steady conditions can be achieved for wind speeds ranging from approximately 0·6 m/s to about 9·5 m/s.

The entire wind-wave generation system is mounted directly on the laboratory floor and not on the wave tank itself. The wave tank and wind-wave system are extremely well isolated from one another, their only points of contact being flexible rubber seals which provide the air seal between them. In addition, the programmable wave maker is mounted on the wind-wave system and is, therefore, also mechanically isolated from the wave tank.

A simplified block diagram of the X-band radar system is shown in figure 2. The system consists of a two-loop stabilized transmitter, which transmits coherent cw power at a frequency of 9·23 GHz, and a superheterodyne receiver which can separately detect amplitude and phase information in the return microwave signal. The local-oscillator Klystron is stabilized by means of a phase-lock loop to a microwave synchronizer. The transmitter Klystron is stabilized and phase-locked to the local-oscillator Klystron at a crystal-stabilized offset frequency of 30 MHz.

In the monostatic backscattering mode used here, the transmitter power is routed

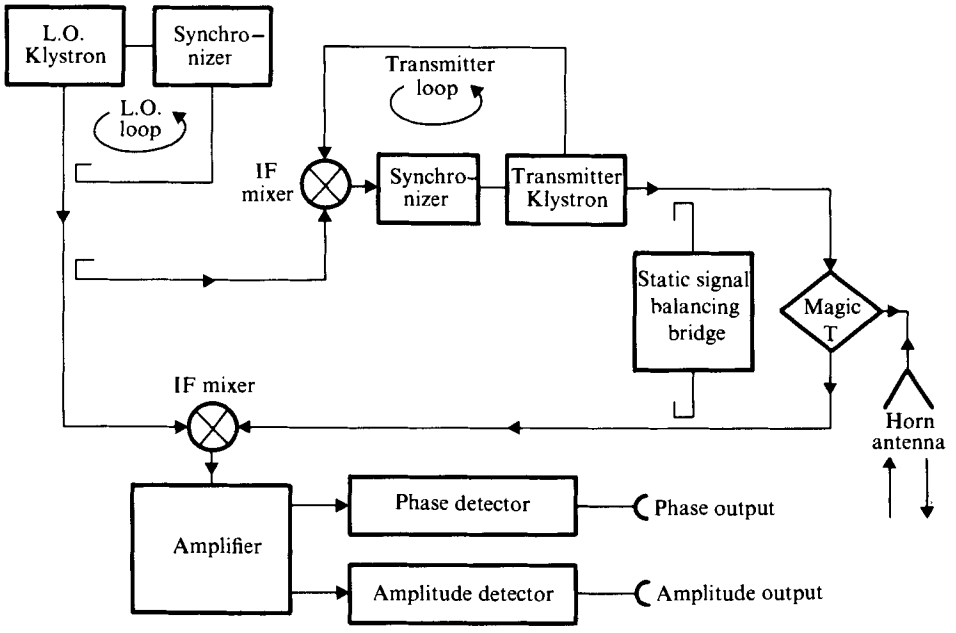

FIGURE 2. Block diagram of superheterodyne X-band radar system. Transmitting frequency is 9·23 GHz.

through a Magic-T to the horn antenna and radiated. The backscattered power is routed through the Magic-T towards an IF mixer where the backscattered microwave signal is mixed with the local-oscillator signal. This resultant IF signal is then logarithmically amplified and its phase and amplitude separately detected. Direct leakage through the Magic-T or via other devious paths and static signals, reflected or scattered from stationary objects, is balanced by a deliberate mismatch of one Magic-T arm by means of an *E–H* tuner, as well as by use of a static signal balancing bridge.

The antenna support system consists of a solid mount for the horn antenna. The antenna is provided with translational and rotational degrees of freedom, which are power driven by d.c. motors. The whole system is mounted in a rigid frame which can be moved to different positions along the top of the wind tunnel, where a section of the wind-tunnel ceiling is removed and replaced by a clear sheet of polyethylene. This permits passage of the microwave beam with minimum beam attenuation and no disturbance to the air flow in the wind tunnel.

The experimental configuration can be seen in figure 1. The wind speed is denoted by U, the fetch by x. The incidence angle θ_i is the angle between the mean surface normal and the antenna boresight. In this paper, only upwind-looking incidence angles have been used.

The distance between the antenna and the water surface along the antenna boresight is always chosen large enough (~ 3 m) so that the illuminated region of the water surface is in the far field of the horn antenna. All of the experiments are performed with an X-band standard gain horn (aperture 19·4 × 14·4 cm, length 30·5 cm), which has a 3 dB beam width of about 11° in both the E and the H plane for a transmitting frequency of 9·23 GHz. The size of the illuminated spot is controlled by an aperture

(figure 1). The aperture board is 245 cm long (or longer if required), 93 cm wide (which covers the width of the wave tank) and 3·6 cm thick. It is covered with microwave absorbing material. A 60 × 60 cm square hole is cut out in the middle of the board; this defines the area of the illuminated spot. The bottom of the board is 4 cm above the water surface.

3. Experimental procedure and results

The Bragg scatterers under study are wind-generated ripples of wavelength approximately 2 cm, i.e. gravity–capillary waves. From the first-order Bragg condition for backscatter

$$\lambda_B = \lambda_0/2 \sin \theta_i, \tag{1}$$

where λ_B is the Bragg resonant wavelength of the water wave, λ_0 is the microwave wavelength and θ_i is the incidence angle, one notes that, for a fixed λ_0, there is a one-to-one correspondence between the incidence angle and Bragg resonant wavelength. In other words, the radar is in a sense a spectrometer, since any water wavelength from the wind-wave spectrum can be selected for detection by the appropriate choice of incidence angle. This fact is demonstrated in an example shown in figure 3 (plate 1), which shows Doppler spectra obtained at a 7·5 m fetch from a 3 m/s wind-wave field for various incidence angles. In this figure, the peaks in the spectra below 1 Hz are due to radar tuning. The peak at ~ 6 Hz is due to specular reflexion from the dominant wave, and the peaks at 13–20 Hz are the Doppler-shifted frequencies corresponding to ripples of different wavelengths between 2·53 and 1·88 cm. In this case, the incident microwavelength is 3·25 cm. For the present investigation, incidence angles of 45°, 50° and 55° have been used to study the effect of gravity waves on radar returns from Bragg waves of wavelengths between 2·3 and 1·98 cm.

Microwave measurements were made at nominal fetches of 4·73 m and 7·15 m. Actual fetches are 7·6–11 cm shorter than the nominal value, depending on the incidence angle. Only the vertical polarization state was used.

Wind speeds were measured with both a hot-wire anemometer and a Pitot probe located in the wind tunnel at a fetch of 9·15 m at a height above the water surface of 40 cm (hot wire) to 50 cm (Pitot probe).

A capacitance surface-wave amplitude gauge of the type used by McGoldrick (1970) was located at the same nominal fetch as the microwave measurement station, but was outside the aperture-controlled illuminated spot.

The steepness of the mechanically generated gravity waves is denoted by ka; this was measured at the test section where the microwave measurements were made.

Doppler spectra from the microwave phase channel were obtained from a real-time time-compression spectrum analyser (Honeywell-SAICOR 51 B). Each recorded spectrum results from a typical sampling/averaging time of 125 s. The vertical scale of the spectrum is the logarithm of the squared input signal, in which 0 dB output refers to a 100 mV r.m.s. sine-wave input. The horizontal (frequency) scale is linear, with a frequency resolution of 0·25 Hz for 50 Hz full scale.

From the microwave signals, the phase channel yields the Doppler spectrum, from which the speed of the Bragg wave can be deduced using the Doppler frequency. The backscattered power can be obtained from the microwave amplitude signal. The backscattered power is not the topic of interest in this paper and will not be discussed. It

should be pointed out that the Doppler spectrum obtained from the superheterodyne receiver used here differs from the Doppler spectrum obtained from the commonly used autodyne (or homodyne) receiver. In the autodyne receiver the output is the product $A(t)\cos\phi(t)$, where $A(t)$ is the amplitude and $\phi(t)$ is the phase of the back-scattered signal. The superheterodyne receiver, however, permits separation of the amplitude and phase information by obtaining $A(t)$ through rectification and envelope detection of the IF output and by obtaining $\cos\phi(t)$ by phase comparison after limiting.† The time derivative $\phi'(t)$ of the phase is the angular Doppler frequency.

The Doppler frequency f_D is related to the speed v of the Bragg scatterer by

$$f_D = (2v/\lambda_0)\sin\theta_i. \tag{2}$$

From the Bragg condition, (2) reduces to

$$f_D = v/\lambda_B. \tag{3}$$

In an ideal case, the frequency spectrum of $\cos\phi(t)$ would yield a line at the corresponding Doppler frequency ($f_D = \phi'/2\pi$). However, owing to the finite scatterer lifetime (i.e. the dissipative nature of ripples), fluctuation of the Bragg wave speed about a mean value, and second-order electromagnetic and hydrodynamic effects (Johnstone 1975), the Doppler 'line' is usually considerably broadened. In the present study, the Doppler frequency is indicated by the peak of the Doppler spectrum. This Doppler frequency is then related through (3) to the mean speed of the Bragg wave.

From the Doppler spectra, it is observed that the presence of a gravity wave has the effect of increasing the Doppler frequency of the wind-generated ripple. An example of typical Doppler spectra obtained at a 7·15 m fetch is shown in figure 4 (plate 2). In this case, the gravity wave's frequency is 2·25 Hz, which corresponds to a wavelength of 30·8 cm. The ripples are generated by a 3·88 m/s wind. The ripple wavelengths are 2·3 cm, 2·12 cm and 1·98 cm, which correspond to incidence angles of 45°, 50° and 55°, respectively. For any ripple, the measured Doppler frequency for the case $ka = 0$ (i.e. wind only) translates into a Bragg wave speed which is larger than the phase speed corresponding to the Bragg wavelength, indicating that wind-induced surface currents and other effects have contributed to the Bragg wave speed. One observes that, for a fixed wind speed, the increase in Doppler frequency, relative to the case of no gravity waves ($ka = 0$), is proportional to the steepness of the gravity wave ka. As ka becomes large, the Doppler spectra tend to discretize (e.g. for $ka = 12{\cdot}9$ %). For further increases in ka, a finite amplitude instability sets in and an envelope modulation of the gravity wave occurs; this nonlinear effect is excluded from the present study. One notes from the Doppler spectra in figure 4 that low frequency peaks are also present; these occur at the frequency of the gravity wave (or the dominant wave if $ka = 0$) and its higher harmonics. They are produced by multiple forward scattering caused by the aperture, which results in specular reflexion by the gravity (or dominant) wave, and are not due to Bragg scattering.

The discretization of the Doppler spectrum for large ka is due to hydrodynamic interaction between the gravity wave and the ripples and is not an artifact of the microwave diagnostics. This will become clear in the next section.

† Limiting of the IF signal is achieved by a diode clipper, and phase comparison is accomplished by means of a balanced demodulator which compares the phase of the IF signal with a reference phase derived from a 30 MHz crystal-controlled oscillator.

Another observed effect of gravity waves on wind-generated ripples is that, for the same wave steepness ka, the Doppler shift is higher for a lower frequency gravity wave, i.e. the Doppler shift is proportional to the phase speed c_p of the gravity wave.

The variable surface tilting due to different ka makes the radar select different Bragg waves for a given nominal incidence angle, however this tilt effect on the Bragg condition is small and can be estimated as follows. Differentiating (1) on both sides and using the Bragg condition for the nominal incidence angle one obtains

$$\delta\lambda_B/\lambda_B = -\delta\theta_i/\tan\theta_i, \tag{4a}$$

where λ_B is the Bragg wavelength corresponding to the nominal incidence angle θ_i and $\delta\lambda_B$ is the change in the Bragg wavelength corresponding to the surface tilt angle $\delta\theta_i$, which is equal to arctan ka. Similarly, the change in the Bragg wave frequency corresponding to the tilt can be found from the dispersion relation

$$\omega_B^2 = (gk_B + \sigma k_B^3),$$

where ω_B is the angular Bragg wave frequency, k_B is the Bragg wavenumber $(2\pi/\lambda_B)$, g is the acceleration due to gravity (981 cm/s^2) and σ is the surface tension divided by the density of water (73·5 cm^3/s^2). One thus obtains

$$\frac{\delta\omega_B}{\omega_B} = \left(\frac{1}{2} + \frac{\sigma k_B^3}{\omega_B^2}\right)\frac{\delta\theta_i}{\tan\theta_i}, \tag{4b}$$

where the quantity in the brackets on the right-hand side is smaller than unity for nominal Bragg wavelengths between 1·98 and 2·3 cm. Since in this experiment $ka \lesssim 0{\cdot}1$, the tilt angle is limited to $\delta\theta_i \sim 0{\cdot}1$ rad. Therefore, for nominal incidence angles between 45° and 55°, the maximum deviation of a Bragg wavelength from its nominal value is not more than 10 %.

From the above observations, it is natural to conclude that the increase in Bragg wave speed (relative to the case of no gravity waves) is proportional to the slope and phase speed of the gravity wave, or some function thereof. Since the measured increase $\Delta f_D \lambda_B$ in Bragg wave speed is larger than the Stokes drift (Longuet-Higgins 1953) $2k^2a^2c_p$ by an order of magnitude, one is led to assume that

$$\Delta v \equiv \Delta f_D \lambda_B = ka\, c_p(1 + 2\,ka), \tag{5}$$

where $\Delta f_D = f_D - f_{D0}$, f_{D0} being the measured Doppler frequency for the case $ka = 0$. Dividing (5) by c_p, one obtains the normalized increase in Bragg wave speed as a function of the slope of the gravity wave. The experimental data normalized in this fashion are plotted in figure 5. It can be seen from this figure that (5) fits the data very well. The somewhat larger scatter exhibited by the data points for a 4·73 m fetch is due to the fact that instantaneous values of ka, instead of average values of ka, are used for data reduction purposes. The scatter in the data points for a 7·15 m fetch is much smaller by comparison, since only long-time (t = 30 s) average values of ka are used. The amplitude a of the gravity wave plus whatever effect the wind had on the amplitude was measured by the co-located capacitance wave gauge. The gravity wave's wavenumber k was computed from the appropriate dispersion relation with the specified frequency of the gravity wave.

The remarkable fact indicated by the experimental data is that Δv is of the order of the orbital speed kac_p of the gravity wave and not of the order of the Stokes drift,

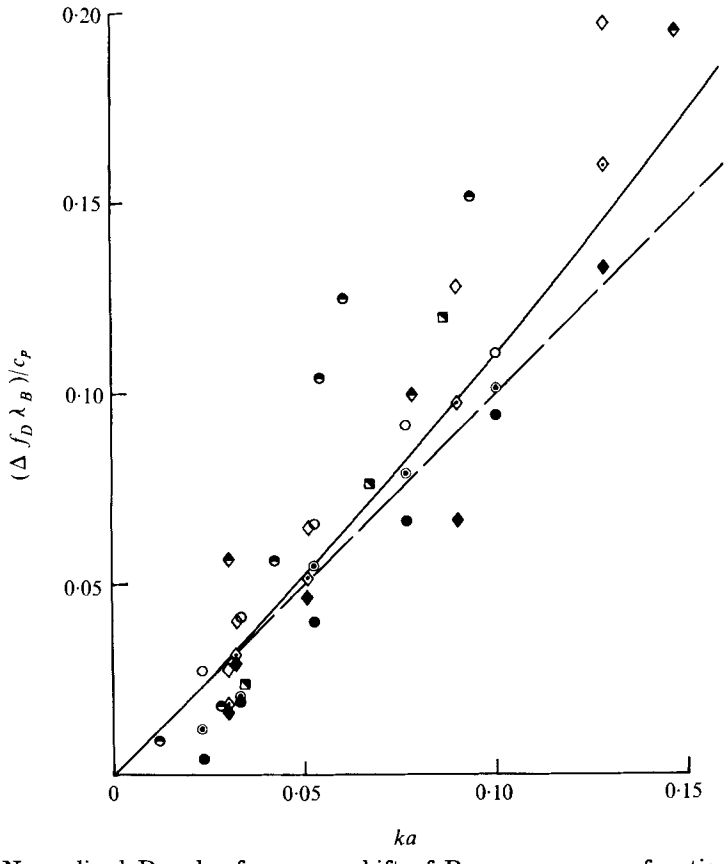

FIGURE 5. Normalized Doppler frequency shift of Bragg wave as a function of steepness of gravity wave. – – –, orbital speed of gravity wave; ——, orbital speed of gravity wave plus Stokes drift [equation (4)]. (*a*) x = 4·73 m, U = 3·7 m/s, (*b*) x = 7·15 m, U = 3·88 m/s. Data at 4·73 m fetch exhibit larger scatter because instantaneous wave amplitudes instead of average values are used for data reduction.

(*a*) θ_i/f 55°/1·5 Hz 55°/1·75 Hz 55°/2·25 Hz

(*b*) θ_i/f 45°/1·5 Hz 50°/1·5 Hz 55°/1·5 Hz 45°/2·25 Hz 50°/2·25 Hz 55°/2·25 Hz

which is only a few per cent of kac_p. This fact strongly suggests that, through the interaction of the gravity wave with the ripples, the Bragg waves (e.g. ripples) are concentrated predominantly around the crests of the gravity wave so they have a maximum speed contribution due to orbital motion in the positive direction.† If this were not the case and the Bragg scatterers were distributed randomly over the gravity wave, then on the average it would be equally possible for the Bragg scatterers to be at all locations on the gravity wave. The Bragg scatterers in the trough would give a contribution from the gravity wave's orbital speed that would be opposed to the wind-induced surface current. The net effect of the gravity wave on the measured Bragg wave speed would

† Banner & Phillips (1974) have shown that there is a nonlinear augmentation of the surface drift near the gravity wave's crest. The augmented drift is calculated to be also only a few per cent of the gravity wave's orbital speed in the present case. Within the data scatter, the contribution of the augmented drift is indistinguishable from that of the Stokes drift.

then be a further spectral broadening (of the Doppler spectrum for the case $ka = 0$) due to positive and negative contributions from the crests and troughs of the gravity wave, respectively, and perhaps also a small Doppler shift corresponding to the Stokes drift. That this is not so and that (5) fits the experimental data very well leads one to hypothesize that the Bragg scatterers are predominantly located on the crests of the gravity wave.

In order to validate this hypothesis, experimental verification that the Doppler returns were indeed obtained from the crest portions of the gravity wave is required. In the present case, the gravity wave's frequency is between 1·5 and 2·25 Hz, the size of the illuminated spot (60 cm) is of the order of the gravity wave's wavelength or larger, and microwave returns from any specific portion of the gravity wave cannot be distinguished. In the next section, a conditional sampling technique which permits sampling of microwave signals from any portion of the gravity wave is applied. The result of the experiment using the conditional sampling technique not only provides an answer to the question posed, but also explains the observed phenomenon of the discretization of the Doppler spectrum for gravity waves of large steepness.

4. Conditional sampling

Procedure and results

The basis of the conditional sampling technique involves the sampling of the microwave signals returned from any particular portion of the gravity wave. Since the gravity wave is continuous, and the radar operates in a cw mode, the way to execute the conditional sampling technique is to restrict the size of the illuminated spot such that only a small portion of the gravity wave is illuminated and therefore contributes to backscattering. The microwave returns can then be sampled at times when a certain portion of the gravity wave is exposed in the small aperture. This is effected by the use of a triggered sampling pulse and a multiplier which multiplies the cw microwave signal and the sampling pulse signal. The output from the multiplier is then spectrum analysed in the usual manner.

The sampling pulse is triggered by a low-pass filtered wave amplitude signal from a wave gauge located at a 7·15 m fetch. Low-pass filtering is applied to remove high frequency wind-wave contributions, thus revealing a 'clean' gravity wave signal for triggering purposes. The sampling pulse can be adjusted for a range of desired delay times; this allows for the 'positioning' of the sampling pulse on any part of the gravity wave. The repetition rate of the sampling pulse can be adjusted to 1, $\frac{1}{2}$ or $\frac{1}{3}$ of the gravity wave's frequency. The pulse width is also adjustable.

The spatial resolution $\Delta\lambda$, i.e. the smallest portion of the gravity wave from which sampling of the Doppler signal can yield meaningful results, is limited by the aperture width b and the pulse width ΔT. This can be written as follows:

$$\Delta\lambda = \Delta T c_p + b, \tag{6}$$

where c_p is the phase speed of the gravity wave.

There are limitations on both b and ΔT. The aperture width has to be at least larger than a few Bragg wavelengths and is quite obvious since Bragg scattering is essentially scattering from an array of scatterers (i.e. Bragg waves). The aperture width should

also be much larger than the incident microwave wavelength in order to allow plane electromagnetic waves passing through it to remain plane. The latter condition need not be too stringently imposed in the present case since the aperture board is situated quite close to the water surface. The pulse width should be larger than a few Doppler periods (i.e. $\Delta T > 1/f_D$), since in order to have a reasonable spectrum, many Doppler oscillations within one pulse 'window' are desired.

An expression for the fractional resolution $\Delta\lambda/\lambda$ can be obtained by division of (6) by λ, the gravity wave's wavelength. It can be seen that the best achievable fractional resolution is also limited by the longest gravity wave the wave paddle can generate.

For conditional sampling, an aperture board with a 10×50 cm opening is used, the narrow dimension being in the fetchwise direction. The fractional resolution is between 0·25 and 0·33, depending on the choice of ΔT and λ. It should be pointed out that a fractional resolution smaller than 0·5 would be sufficient for the present purpose.

In what follows, the centre of $\Delta\lambda$ will be defined as the sampling location on the gravity wave. This sampling location will be denoted by a phase angle ψ, where 0° refers to the forward node, 90° refers to the crest, 180° refers to the backward node and 270° refers to the trough of the gravity wave.

Typical conditionally sampled Doppler spectra of a gravity wave ($f = 1{\cdot}561$ Hz) and a wind wave ($U = 3{\cdot}93$ m/s) for different slopes of the gravity wave are shown in figure 6 (plate 3). The sampling-pulse repetition rate is $\frac{1}{2}f$, i.e. every other gravity wave is sampled; the pulse width is 0·118 s. Each Doppler spectrum is obtained with an averaging time of 112 s. This means that only 87·4 gravity waves are actually sampled, and because of the pulse width, the net sampling time is only 10·3 s. High-pass filtering of the microwave signal at 2Hz was used to reduce the spectral peak occurring at the frequency of the gravity wave (the appearance of which has been explained in § 3) in order to keep the total spectral amplitude within the dynamic range of the spectrum analyser.

From figure 6, one observes quite unambiguously that the Doppler spectrum of the Bragg wave ($f_D > 19{\cdot}2$ Hz) peaks at 90° for all values of ka, indicating that the Bragg scatterers are located predominantly at the crests of the gravity wave (spectral peaks which occur at frequencies below 15 Hz are sampling-pulse artifacts). Note, however, that 'crest' means a location centred at 90° or $\pm 45°$ (or up to $\pm 60°$) depending on the fractional resolution, and likewise for other locations. One further notes that for small wave slopes (e.g. $ka = 2{\cdot}4\,\%$), there are Bragg scatterers located at the nodes as well, and perhaps even in the troughs. But as ka increases, the back nodes (180°) and troughs (270°) of the gravity wave are gradually depleted of Bragg scatterers, and finally, at the largest ka, there are Bragg waves only at the crests. The small 'bumps' in the Doppler spectra for the case $ka = 11{\cdot}2\,\%$ are due to the envelope of the spectrum of the sampling pulse (this will be discussed further), indicating that there are no Doppler oscillations (i.e. no Bragg scatterers) within those pulses sampled at locations away from the crests.

The tendency of Bragg waves (ripples) to become progressively 'localized' as the gravity wave's slope increases can also be observed from the illustrative example of oscillograph records shown in figure 7. In this figure, the radar Doppler signal and the wave amplitude signal (of the capacitance wave gauge) are shown for the same case as the previous example. Note that when the gravity wave is absent ($ka = 0$) Doppler bursts occur in a random fashion. As ka increases, the Doppler bursts become more and more localized. The occurrence of the bursts not only becomes quite regular, but the

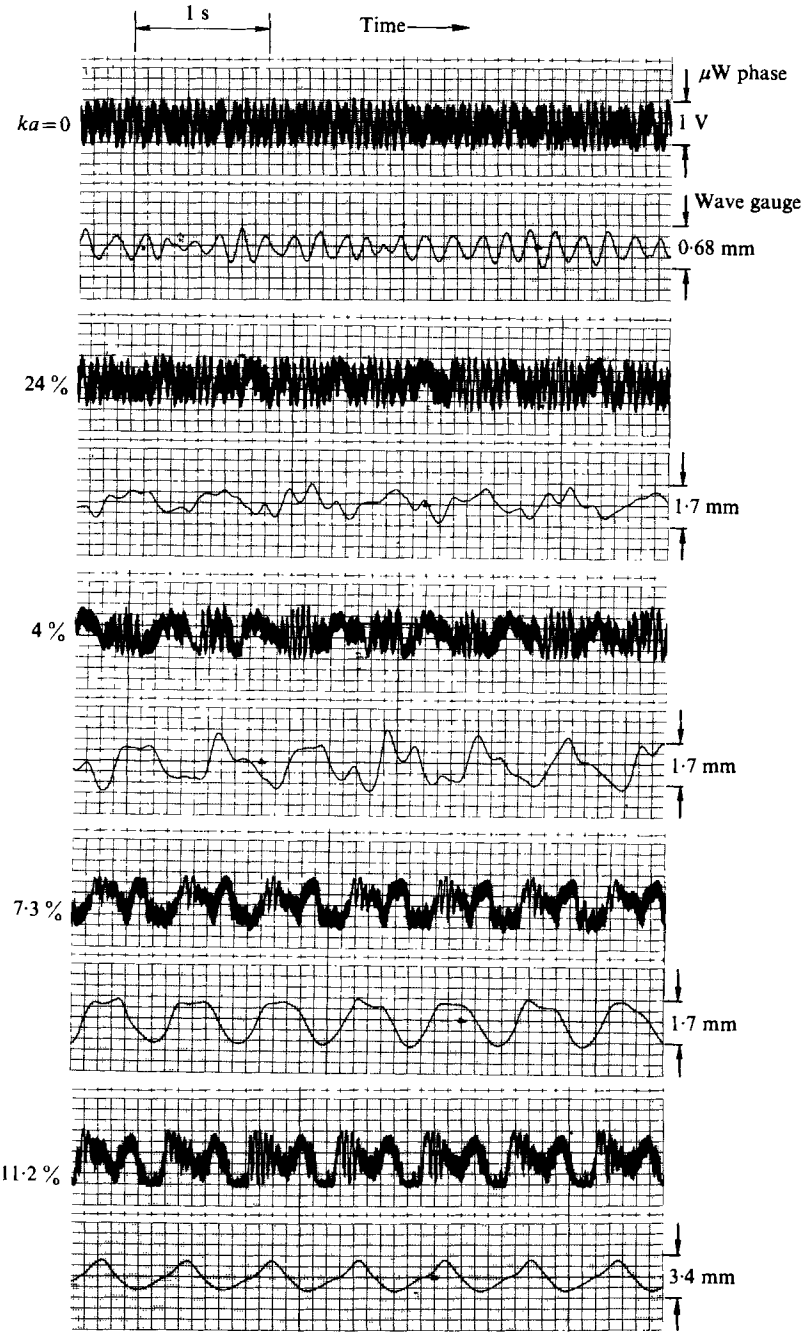

FIGURE 7. Typical oscillograph traces of microwave phase (i.e. Doppler) signals and wave amplitude signals of wind wave (U = 3·93 m/s) on gravity waves (f = 1·5613 Hz) of different steepness. Note that Doppler bursts (i.e. oscillations with frequency of ~ 19 Hz or higher) occur randomly when the gravity wave is absent, but that their occurrence becomes more regular with increasing steepness of the gravity wave. The Doppler bursts actually occur on the gravity wave's crests. The apparent phase shift between the locations of Doppler bursts and the gravity wave's crests occurs because the antenna boresight intercepts the mean water surface 11 cm upstream of the wave gauge. Therefore the Doppler signal leads the wave amplitude signal.

	f_D(Hz)	
ka	Measured (figure 5, 90°)	Computed [equation (5)]
0·024	20	20·47
0·040	21	21·38
0·073	22·5	23·42
0·112	26·5	26·11

TABLE 1. Comparison between Doppler frequencies measured at crests of gravity wave and computed from (5).

bursts are located at the crests of the gravity wave. The apparent phase shift between the Doppler burst locations and the wave crests in the oscillograms is due to the fact that the antenna boresight intersects the mean water surface at a 7·04 m fetch (for $\theta_i = 55°$) while the wave gauge is located at the nominal 7·15 m fetch. The microwave senses the crest approximately 0·1 s before the wave gauge because it is 11 cm upstream of the wave gauge and the gravity wave's phase speed is 100 cm/s in the present case.

Incidentally, the Doppler frequencies measured at the crests of the gravity wave for various wave slopes compare very well with Doppler frequencies computed from (5) for these wave slopes. The results for the example shown in figure 6 are given in table 1. Here the pertinent values are $c_p = 100$ cm/s, $\lambda_B = 1{\cdot}983$ cm and $f_{D0} = 19{\cdot}2$ Hz.

An explanation for the discretization of the Doppler spectrum

From the experimental evidence described above, one can conclude that through interaction with the gravity wave the Bragg scatterers tend to be progressively 'localized' at the crests of the gravity wave and that the occurrence of Doppler bursts becomes more regular with increasing slope of the gravity wave.

The above conclusion in essence explains why the Doppler spectrum becomes discretized for gravity waves of large slope. As the slope of the gravity wave becomes large, the Doppler bursts occur regularly at fixed intervals equal to the period of the gravity wave (see figure 7). This, however, is equivalent to a periodic pulse train of Doppler bursts synchronized at the gravity wave's frequency. The discrete lines in the Doppler spectrum are therefore due to the 'form' wave contributed by the pulse envelope.

To elucidate this point further, consider the spectrum of a rectangular pulse train of unit height, period p and pulse width ΔT. The power spectrum of such a pulse train has the following characteristics: (i) the spectrum lines are separated by an interval $1/p$, i.e. the pulse frequency, and (ii) the envelope of the spectrum is zero at $f = 1/\Delta T$ and integral multiples thereof. In other words, as p becomes larger, i.e. as the pulse period becomes longer, the envelope of the spectrum appears to be smoother because the spectrum lines are closer together. The apparent smoothing occurs because the spectrum analyser does not have infinite resolution in frequency.

As an example the spectra of rectangular pulses with the same pulse width but different periods are shown in figure 8(*a*) (plate 4). In case 1, the pulse frequency is 1·5613 Hz; in case 2, the pulse frequency is 0·7806 Hz. In both cases the pulse width is 0·1345 s. As can be clearly seen from this figure, the pulse train with the longer period

(case 2) has a smoother spectrum. Also it can be noted from case 1 that the separation between spectrum lines is 1·56 Hz, which is the pulse frequency. If one uses these two rectangular pulse trains as sampling pulses to conditionally sample the Doppler signals for measurement conditions of the type used in the experiments of figures 6 and 7, then one obtains the Doppler spectra (sampled at gravity wave crest) shown in figure 8(*b*) (plate 4). The Doppler spectrum sampled every gravity wave appears with discrete spectrum lines (case 1). The Doppler spectrum sampled every other gravity wave is much smoother (case 2).

Figure 4 can now be re-examined, and it is found that the discrete Doppler lines are separated by 2·25 Hz, which is the frequency of the gravity wave. Also, from figure 6, the artifacts in the Doppler spectra, which are due to the sampling pulse train, now become quite evident and clearly identifiable when the spectra in figure 8(*a*) are consulted.

5. Discussion

It has been found that when gravity waves interact with wind-generated ripples a Doppler shift corresponding to an increase in the ripple speed can be detected via microwave Bragg backscattering. The Doppler shift corresponds, to first order, to the gravity wave's orbital speed kac_p. Furthermore, it has been shown experimentally, using a conditional sampling technique, that the interaction of a gravity wave with wind-generated ripples leads to 'localization' of the ripples at the gravity wave's crests. This localization of the ripples at the gravity wave's crests increases with increased steepness of the gravity wave. This not only accounts for the observed magnitude of the increase in ripple speed, but also provides an explanation for the observed discretization of the Doppler spectra measured when the gravity wave becomes steep. The explanation for the discretization of the Doppler spectra has been further elucidated by an experimental verification.

The exact mechanisms leading to the observed phenomenon are not known. However, Keller & Wright (1975) have studied the modulation in backscattered microwave power from wind-generated ripples (of wavelength 2·3 cm) induced by the presence of a long (wavelength = 420 cm) gravity wave. Their analysis, which attributes the modulation to wind relaxation, radiation stress (Longuet-Higgins & Stewart 1960) and the tilt effect, predicts that the modulated microwave power is localized at positions leading the crests of the gravity wave, the lead angle depending on hydrodynamic parameters, the relaxation time and the air friction velocity. A calculation of the lead angle, using the linear theory of Keller & Wright, was performed for the conditions of the present experiments. The results of the hydrodynamic model indicate that the location of the maximum in the wave-height spectrum at the Bragg wavenumber is $\sim 20°$ ahead of the crest. If the microwave tilt effect were included in estimating the lead angle of the microwave signal, the theoretical value would be $\sim 40°$. In the present measurements, the Doppler signal is only slightly sensitive to the tilt effect; therefore the Keller & Wright theory indicates that the maximum signal will occur somewhere between 20° and 40° from the crest. The present data indicate, however, that the lead angle is between 0° and 20°.

The ripples, which in the present study have wavelengths between 2·3 and 1·98 cm, have phase velocities close to the minimum phase speed of deep-water waves; therefore

their generation is most likely to be due to shear instability. According to an explanation given by Munk (1955), the stable position for ripples is on the leading slope (i.e. at the 0° position in the notation of this paper) of the dominant gravity wave because of the zone of convergence created by the gravity wave's orbital velocity. The results, however, do not indicate that this explanation is correct.

The theory on the interaction of short waves and long waves of Longuet-Higgins & Stewart predicts that the short waves become shorter and steeper at the crests of the longer waves, and correspondingly longer and less steep in the troughs of the longer waves. For deep water, which corresponds to the present experimental conditions, the expressions are

$$a'_B/a_B = 1 + ka\sin\psi, \tag{7a}$$

$$k'_B/k_B = 1 + ka\sin\psi, \tag{7b}$$

where ka is the slope of the longer wave, ψ is the phase angle (90° corresponds to crest) and a_B and k_B, the Bragg wave amplitude and wavenumber, respectively, are the mean values of a'_B and k'_B, respectively. The changes in the short wave's amplitude and wavenumber therefore vary between $1+ka$ and $1-ka$. For the gravity wave slopes encountered in the present experiments, the deviations in both ripple amplitude and ripple wavelength are not more than approximately 10 % about the mean (or nominal) value. Consequently, if there were a certain Bragg wave uniformly distributed over the gravity wave, the fact that the lengthening and flattening of the Bragg wave in the trough of the gravity wave are less than 10 % would not render them undetectable by the radar. The results of the conditional sampling, however, indicate that even at $ka \sim 0{\cdot}07$ there are no radar returns from the troughs of the gravity wave; this means that in the troughs the Bragg waves have already been wiped out or at least greatly reduced in amplitude (i.e. by much more than 7 %). This can probably be ascribed to the fact that, because of the presence of wind, ripple generation becomes a local phenomenon as well. The presence of wind was not considered in the Longuet-Higgins & Stewart theory. The increase in the Bragg wave amplitude with ka was not compared with the theory for the present experiments for the following reason: in order to get amplitude measurements of the Bragg waves, one needs to measure the backscattered power, which can be related to the radar scattering cross-section. The scattering cross-section is related to the Bragg wave height if the Bragg wave is uniform and infinite in spatial extent. The difficulty encountered in the present case is that the Bragg waves are patchy because they are wind generated. Therefore, for a given measured backscattered power, one is not able to distinguish whether it is due to, say, three steep Bragg waves or five less steep ones. However, the present results do not contradict the theory, since it predicts that the crest would provide the most backscattered power owing to a shortening and steepening of the Bragg wave; the former would cause the number of Bragg waves per unit length to increase and the latter would increase the scattering cross-section.

Cox (1958) has also observed, by means of an optical slope gauge, that the location of high frequency ripples is associated with the leading slopes of the low frequency dominant wave for high winds at short fetch. He also noted the generation of ripples on the crests and leading slopes of a plunger-generated wave modified by wind at short fetch. Although Cox stated that the short ripples should precede the long ones, he did not state explicitly what the wavelength of the ripple should be at what position on a

gravity wave. The general results obtained in this paper are, however, not in contradiction with Cox's observations.

In the present experiments, surface statistics were also measured by means of a laser slope gauge. It was found that the characteristic short waves can be quite steep ($ka \sim 0{\cdot}1$–$0{\cdot}15$), indicating that nonlinear effects of the Bragg waves may also play a role in the modulation and localization of the ripples (H. C. Yuen 1976, private communication). However, a detailed assessment of the relative importance of radiation stress, wind relaxation and nonlinear effects is beyond the scope of the present study.

The author is deeply indebted to Dr Bruce Lake, Dr Henry Yuen and Dr Irwin Alber for many helpful discussions, and to Professor E. H. Hsu of Stanford University for suggesting conditional sampling of the microwave signals. This research was supported by the Applied Physics Laboratory of The Johns Hopkins University under Contract APL/JHU no. 600093.

REFERENCES

BANNER, M. L. & PHILLIPS, O. M. 1974 On the incipient breaking of small-scale waves. *J. Fluid Mech.* **65**, 647–657.

BASS, F. G., FUKS, J. M., KALMYKOV, A. I., OSTROVSKY, I. E. & ROSENBERG, A. D. 1968 Very high frequency radiowave scattering by a disturbed sea surface. Parts I and II. *I.E.E.E. Trans. Antennas Propagation* **16**, 554–568.

COX, C. S. 1958 Measurements of slopes of high frequency wind waves. *J. Mar. Res.* **16**, 199–225.

CROMBIE, D. D. 1955 Doppler spectrum of sea echo at 13·56 Mc./s. *Nature* **175**, 681–682.

DUNCAN, J. R., KELLER, W. C. & WRIGHT, J. W. 1974 Fetch and wind dependence of Doppler spectra. *Radio Sci.* **9**, 809–819.

JOHNSTONE, D. 1975 Second-order electromagnetic and hydrodynamic effects in high-frequency radio-wave scattering from the sea. Ph.D. thesis, Stanford University.

KELLER, W. C. & WRIGHT, J. W. 1975 Microwave scattering and the straining of wind-generated waves. *Radio Sci.* **10**, 139–147.

LEWIS, J. E., LAKE, B. M. & KO, D. R. S. 1974 On the interaction of internal waves and surface gravity waves. *J. Fluid Mech.* **63**, 773–800.

LONGUET-HIGGINS, M. S. 1953 Mass transport in water waves. *Phil. Trans. Roy. Soc.* A **245**, 535–581.

LONGUET-HIGGINS, M. S. & STEWART, R. W. 1960 Changes in the form of short gravity waves on long wind waves and tidal currents. *J. Fluid Mech.* **8**, 565–583.

MCGOLDRICK, L. F. 1970 On Wilton's ripples: a special case of resonant interactions. *J. Fluid Mech.* **42**, 193–200.

MUNK, W. 1955 High frequency spectrum of ocean waves. *J. Mar. Res.* **14**, 302–314.

PEAKE, W. H. 1959 The interaction of electromagnetic waves with some natural surfaces. *Antenna Lab., Ohio State Univ. Rep.* no. 898–2.

PIDGEON, V. W. 1968 Doppler dependence of radar sea return. *J. Geophys. Res.* **73**, 1333–1341.

RICE, S. O. 1951 Reflection of electromagnetic waves from slightly rough surfaces. *Comm. Pure Appl. Math.* **4**, 351–378.

SEMYONOV, B. I. 1966 Approximate computation of scattering electromagnetic waves by rough surface contours. *Acad. Sci. U.S.S.R., Rad. Engng Electron. Phys.* **11**, 1179–1187.

UNNA, P. J. 1941 White horses. *Nature* **148**, 226–227.

UNNA, P. J. 1942 Waves and tidal streams. *Nature* **149**, 219–220.

UNNA, P. J. 1947 Sea waves. *Nature* **159**, 239–242.

VALENZUELA, G. R. 1968 Scattering of electromagnetic waves from a tilted slightly rough surface. *Radio Sci.* **3**, 1057–1066.

VALENZUELA, G. R. & LAING, M. B. 1970 Study of Doppler spectra of radar sea echo. *J. Geophys. Res.* **75**, 551–563.

WRIGHT, J. W. 1968 A new model for sea clutter. *I.E.E.E. Trans. Antennas Propagation* **16**, 217–223.

WRIGHT, J. W. & KELLER, W. C. 1971 Doppler spectra in microwave scattering from wind waves. *Phys. Fluids* **14**, 466–474.

YUEN, H. C. & LAKE, B. M. 1975 Nonlinear deep water waves: theory and experiment. *Phys. Fluids* **18**, 956–960.

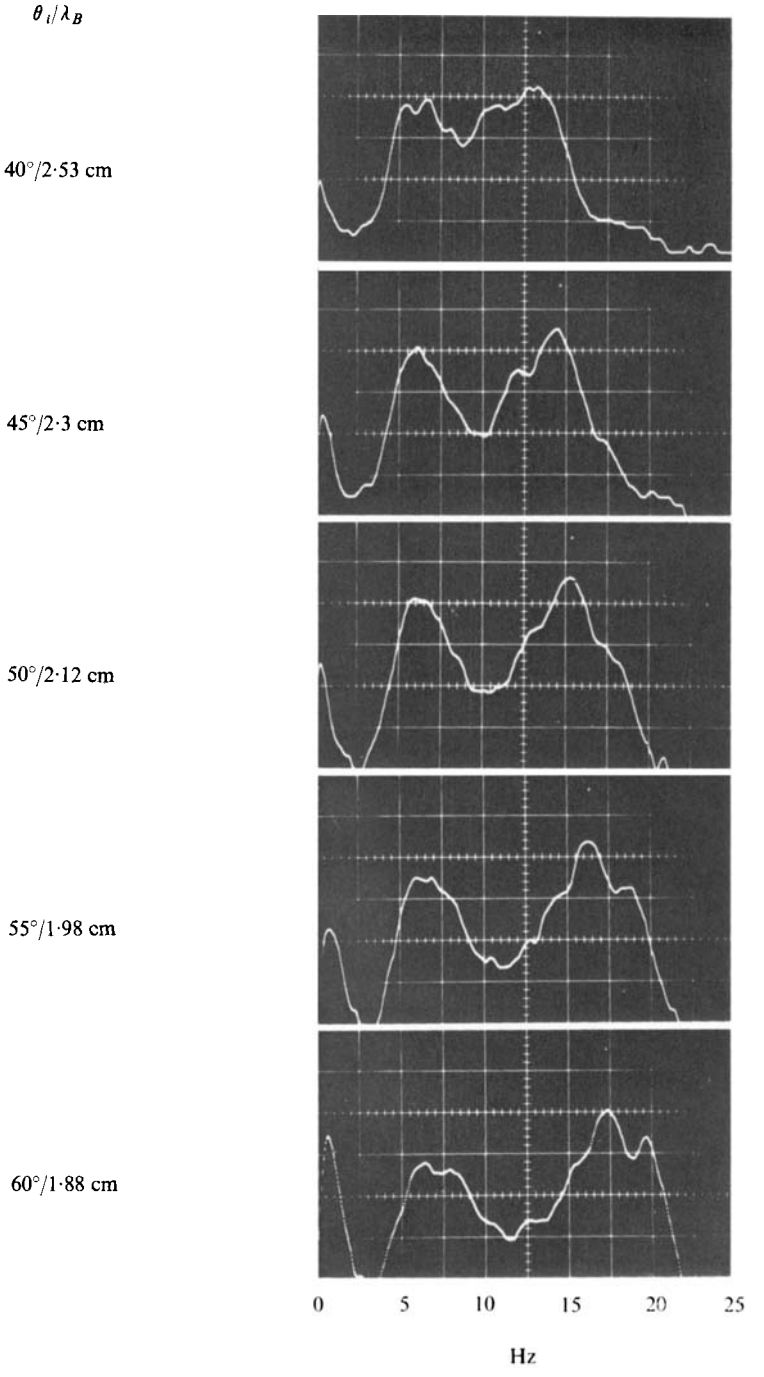

FIGURE 3. Doppler spectra at various incidence angles, which correspond to various Bragg wavelengths, obtained from a wind-wave field (x = 7·5 m, U = 3 m/s). The peak below 1 Hz is due to radar tuning. The peak at ~ 6 Hz is due to the dominant wave. The peaks from 13 Hz to 20 Hz correspond to the Doppler-shifted frequencies of Bragg waves of wavelength between 2·53 and 1·88 cm. Vertical scale 10 dB per division.

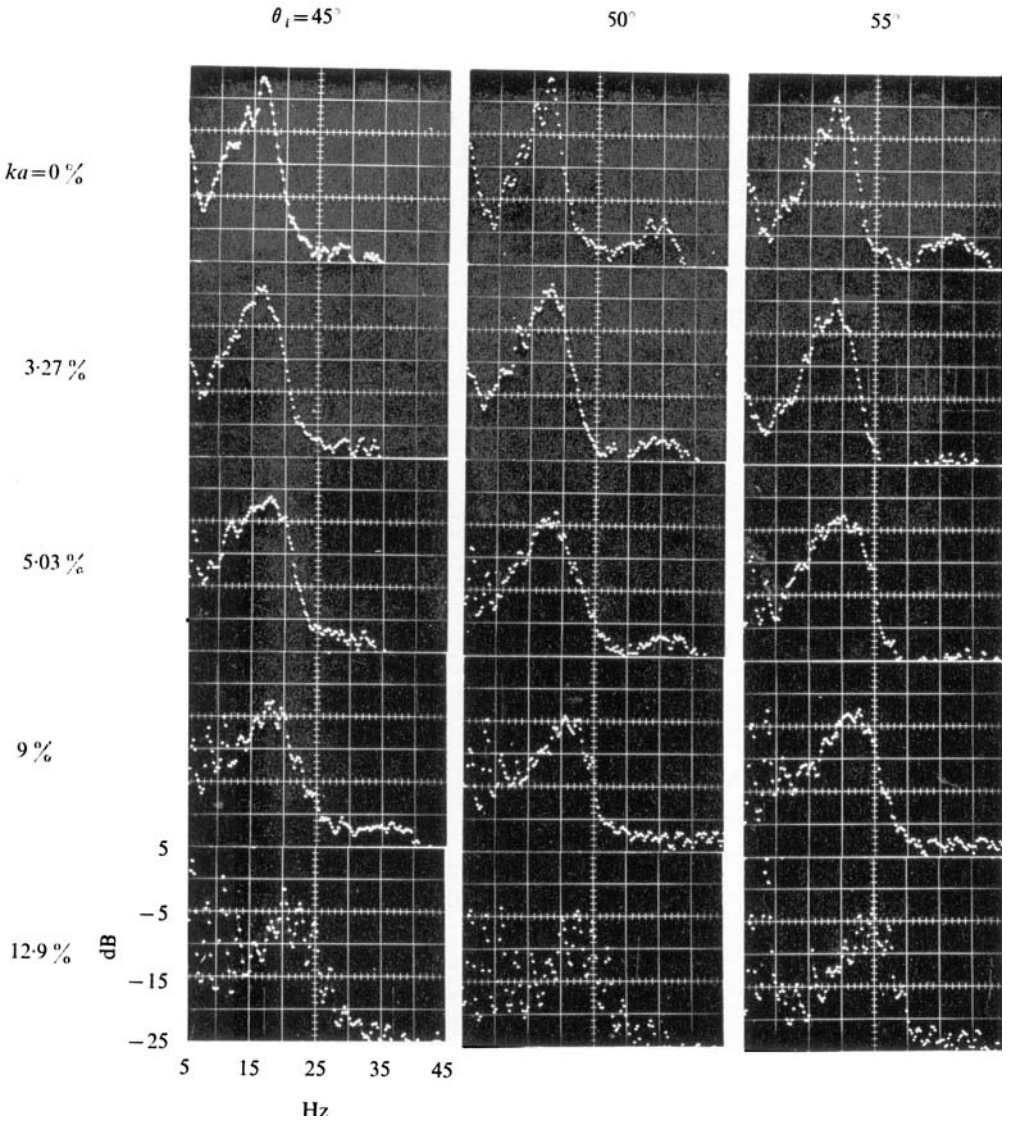

FIGURE 4. Effect of steepness of gravity wave (f = 2·25 Hz) on wind-wave (U = 3·88 m/s) Doppler spectrum. Bragg wavelengths are 2·3, 2·12 and 1·98 cm for incidence angles of 45°, 50° and 55°, respectively. Note discretization of Doppler spectrum for large ka.

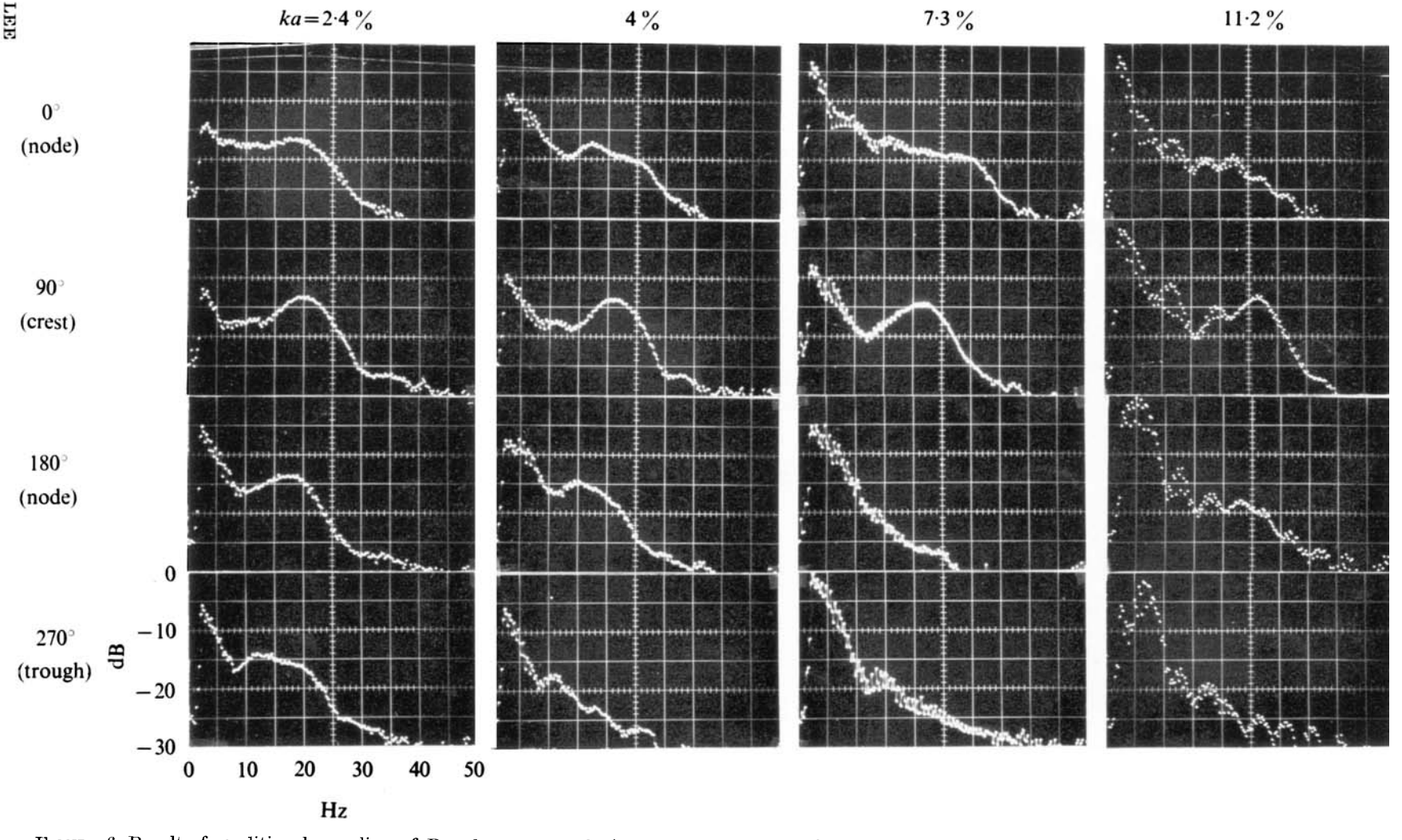

FIGURE 6. Result of conditional sampling of Doppler spectra of wind wave (U = 3·93 m/s) on gravity wave (f = 1·5613 Hz) at 7·15 m fetch. Note that Doppler spectrum peaks at crests of gravity wave, indicating that Bragg scatterers are located predominantly at crests of gravity wave. Spectral peaks ~ 15 Hz below are sampling-pulse artifacts.

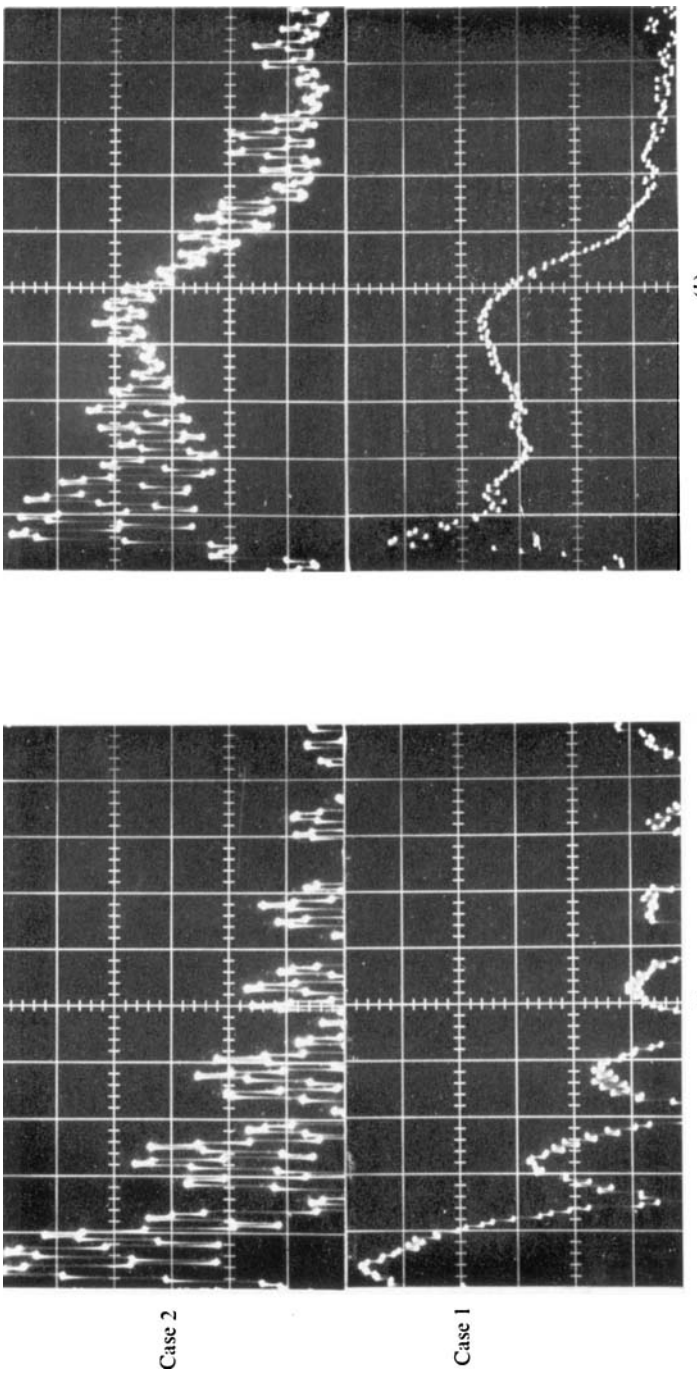

FIGURE 8. Explanation of the discretization of the Doppler spectrum for large ka. (*a*) Spectra of rectangular pulse train with pulse width of 0·1345 s: case 1, pulse frequency (repetition rate) of 1·5613 Hz; case 2, pulse frequency of 0.7806 Hz. (*b*) Doppler spectra conditionally sampled at crests of gravity wave ($f = 1{\cdot}5613$ Hz) with $ka \sim 8\,\%$ and $U = 3{\cdot}93$ m/s. Note that the Doppler spectrum obtained by sampling every other gravity wave is smoother.